

# Synthesis of Zinc Tetraphenylporphyrin Rigid Rods with a Built-In Dipole

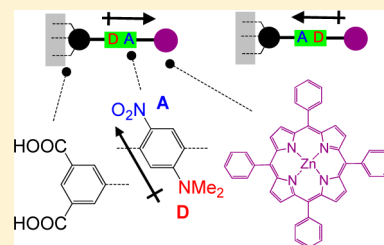
Keyur Chitre,<sup>†</sup> Alberto Batarseh,<sup>†</sup> Andrew Kopecky,<sup>†</sup> Hao Fan,<sup>†</sup> Hao Tang,<sup>†</sup> Roger Lalancette,<sup>†</sup> Robert A. Bartynski,<sup>‡</sup> and Elena Galoppini<sup>\*,†</sup>

<sup>†</sup>Chemistry Department, Rutgers University, 73 Warren Street, Newark, New Jersey 07102, United States

<sup>‡</sup>Department of Physics and Astronomy and Laboratory for Surface Modification, Rutgers University, 136 Frelinghuysen Road, Piscataway, New Jersey 08854, United States

## S Supporting Information

**ABSTRACT:** Three Zn(II) tetraphenylporphyrins (ZnTPP) were synthesized to study the influence of a molecular dipole on the energy level alignment of a chromophore bound to a metal oxide semiconductor: ZnTPP-PE(DA)-IpaOMe (1), ZnTPP-PE-IpaOMe (2), and ZnTPP-PE(AD)-IpaOMe (3). Each contained a rigid-rod linker made of a *p*-phenylene ethynylene (PE) moiety terminated with the methyl ester of an isophthalic acid unit (Ipa). Porphyrins 1 and 3 contained an intramolecular dipole in the central phenyl ring, which was built by introducing electron donor (D, NMe<sub>2</sub>) and acceptor (A, NO<sub>2</sub>) substituents in para position to each other. In 1 and 3, the relative position of the D and A substituents, and therefore the dipole direction, was reversed. Porphyrin 2, without substituents in the linker, was synthesized for a comparison. The structures of precursors to 1 and 3 and the structure of 1 were determined by single crystal X-ray analysis. Solution UV-vis and steady-state fluorescence spectra of 1–3 were identical to each other and exhibited the spectral features typical of the ZnTPP chromophore and their electrochemical properties were also very similar. Methyl esters 1–3 were hydrolyzed to the corresponding carboxylic acids for binding to metal oxide semiconductors.



## 1. INTRODUCTION

Interfaces between organic molecules and transition-metal oxide semiconductors are important for applications ranging from solar cells, to photocatalysts, sensors, and molecular electronics. The alignment of the energy levels between molecules and metal-oxides influences charge transfer and other electronic processes that, in turn, affect the device's performance.<sup>1,2</sup> For this reason there is a widespread effort aimed at controlling and understanding the factors influencing energy level alignment at molecules/semiconductor, as well as other interfaces, such as metals.<sup>3–8</sup> In this context, interface dipoles play an important role and are extensively investigated.<sup>9–13</sup> Molecular dipoles have been used to influence electron transfer across molecule/metal boundaries in experiments that often involved clever molecular design to introduce strong dipoles and to probe the effects of dipole reversals.<sup>14–19</sup> On transition metal oxide semiconductors, the adsorption of structurally simple molecules to form polar layers was found to shift the position of the semiconductor conduction band and influence the open circuit photovoltage and other parameters in dye-sensitized solar cells.<sup>20–26,11,13</sup>

As part of our interest in molecules/semiconductor interfaces, we recently demonstrated that two Zn(II) tetraphenylporphyrins having the structure porphyrin-linker-anchor with a reversible built-in dipole in the linker shift a molecule's energy levels alignment on transition-metal oxide in a predictable manner.<sup>27</sup> The proof-of-concept experiment, which was carried out on a ZnO(11–20) single crystal surface

by UV photoemission spectroscopy (UPS), is illustrated in Figure 1b. A monolayer of molecules with a built-in dipole in the linker and bound to ZnO forms an electrostatic potential that shifts the HOMO and LUMO of the porphyrin chromophore by ( $\pm$ )  $\sim$ 100 meV with respect to the band edges of the semiconductor, when compared to the homologue with no dipole. When the direction of the dipole in the linker was reversed, the shift direction was reversed by the same amount.<sup>27</sup>

Here we describe the synthesis and properties of the dipole-containing porphyrins ZnTPP-PE(DA)-IpaOMe (1) and ZnTPP-PE(AD)-IpaOMe (3) used in that study and shown in Figure 1a. Each contains a phenylene ethynylene (PE) rigid-rod bridge terminated with the methyl ester of an isophthalic acid unit (Ipa), which is an anchoring group used for binding to the semiconductor surface. The more soluble methyl esters 1–3 were used in solution studies and were converted into the corresponding carboxylic acids just prior to binding. Porphyrins 1 and 3 contained an intramolecular dipole in the central PE unit, which was obtained by introducing electron donating (D, NMe<sub>2</sub>) and accepting (A, NO<sub>2</sub>) substituents in the para position to each other. In 1 and 3, the relative position of the D

**Special Issue:** John R. Miller and Marshall D. Newton Festschrift

**Received:** November 11, 2014

**Revised:** January 27, 2015

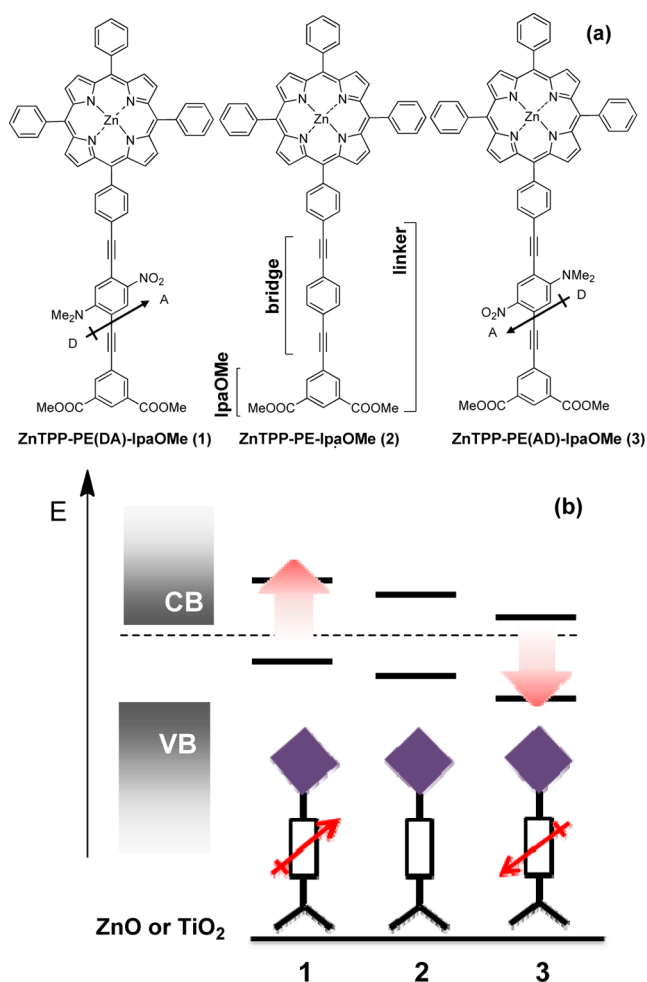


**Figure 1.** (a) Molecular structure of the porphyrins used in the experiment and described here. (b) Schematic diagram of how a dipole in a linker shifts the energy level of a porphyrin chromophore with respect to the conduction band edge of a wide band gap metal oxide semiconductor.<sup>27</sup> The shift direction is indicated by a red arrow.

and A substituents, and therefore the dipole direction, was reversed. Comparisons were made with the previously reported ZnTPP-PE-IpaOMe (2),<sup>28</sup> which is structurally identical to 1 and 3, but that has no substituents, hence no intramolecular dipole in the linker.

The primary requirement for the molecular design of 1, 2, and 3, and the rationale for choosing ZnTPP derivatives, was the ability to introduce an internal dipole in the linker without making significant changes in the size of the HOMO–LUMO gap of the chromophoric unit. This was possible in 1, 2, and 3 because the dipole-containing linker was attached on a mesophenyl group which is nearly orthogonal to the porphyrin plane and therefore electronically decoupled from the macrocycle.<sup>28</sup> Second, the study of 1, 2, and 3 allowed a direct comparison with our previous work on ZnTPP derivatives bound to TiO<sub>2</sub> and ZnO.<sup>28–31</sup> Finally, porphyrin dyes with chromophore-bridge-anchor structures similar to the ones described here have exhibited record efficiencies in photovoltaic applications, are useful models in fundamental charge transfer studies,<sup>32–37</sup> and continue to be of great interest as photocatalysts and in artificial photosynthesis projects.<sup>38–42</sup>

## 2. EXPERIMENTAL SECTION

**2.1. General. Reagents and Methods.** Zn(II) 5-(4-iodophenyl)-10,15,20-triphenylporphyrin (9),<sup>28</sup> dimethyl 5-ethynylisophthalate (5),<sup>28</sup> 2,5-dibromo-4-nitroaniline,<sup>43,44</sup> and ZnTPP-PE-IpaOMe (2)<sup>28</sup> were synthesized according to reported procedures. All commercially available chemicals and solvents were used as received unless otherwise noted. Anhydrous grade, stabilizer-free tetrahydrofuran (THF) was passed through a MBraun solvent purification system immediately prior to use. CH<sub>2</sub>Cl<sub>2</sub> and hexane used for column chromatography were distilled. Ethyl acetate for column chromatography was HPLC grade and used as received. Silica gel plates for thin-layer chromatography (TLC) and silica gel (230–400 mesh) for column chromatography were purchased from Sorbent Technologies. All reactions involving air and moisture sensitive reagents were performed under nitrogen atmosphere in oven-dried or flame-dried glassware and using anhydrous solvents.

**Instrumentation.** <sup>1</sup>H and <sup>13</sup>C NMR spectra were recorded on a Varian INOVA NMR spectrometer operating at 499.896 MHz for <sup>1</sup>H and 125.711 MHz for <sup>13</sup>C using the indicated solvent as an internal reference. Chemical shifts were reported relative to the central line of the solvent: CDCl<sub>3</sub> ( $\delta$  7.26 ppm for <sup>1</sup>H and  $\delta$  77.0 for <sup>13</sup>C spectra) and THF-d<sub>8</sub> ( $\delta$  3.58 ppm for <sup>1</sup>H and  $\delta$  67.60 for <sup>13</sup>C spectra). The coupling constants (*J*) for <sup>1</sup>H NMR are reported in Hertz. High-resolution mass spectra (ESI and MALDI, using 2,5-dihydroxybenzoic acid, 2,5-DBH, as the matrix) were recorded on a Bruker Daltonics Apex-Qe series Fourier Transform Mass Spectrometer. UV–vis absorption spectra were collected on a Varian Cary 500 UV–vis–NIR spectrophotometer at room temperature. Steady-state fluorescence emission spectra were collected on a Horiba Fluorolog-3 instrument equipped with a Xenon short-arc lamp source at room temperature. The excitation wavelength was set to 430 nm with a monochromator bandwidth of 3 nm for both excitation and emission monochromators. UV–vis and fluorescence spectra were corrected by subtracting a baseline spectrum, which was determined for a solution containing all chemicals but porphyrins 1–3. Single attenuated total reflectance infrared (FTIR-ATR) spectra were collected on a Thermo Electron Corporation Nicolet 6700 FT-IR (ZnSe crystal, 128 scans averaged, resolution at 4 cm<sup>-1</sup>).

**Electrochemistry.** Cyclic voltammetry of methyl esters 1–3 was performed on a BAS CV27 potentiostat. The experiments were conducted under nitrogen at room temperature with a conventional three-electrode configuration at a scan rate of 50 mV s<sup>-1</sup>. The data were collected in dichloromethane solutions with a 0.1 M Bu<sub>4</sub>NPF<sub>6</sub> supporting electrolyte. A glassy-carbon working electrode (2 mm diameter) was used along with a platinum wire auxiliary electrode and a Ag wire reference electrode. Ferrocene was used as the internal reference. The half-wave redox potentials (*E*<sub>1/2</sub>) were determined as (*E*<sub>pa</sub> + *E*<sub>pc</sub>)/2, where *E*<sub>pa</sub> and *E*<sub>pc</sub> are the anodic and cathodic peak potentials, respectively. The reduction processes are not reported because of the poor quality of the cyclic voltammetry scans at negative potentials.

**Single-Crystal X-ray Studies.** For each compound, a single crystal was mounted in a Cryoloop using Paratone-N oil. Data were collected at 100 K with the crystal in a stream of N<sub>2</sub> gas on a Bruker APEX2 diffractometer with CCD detector using Cu K $\alpha$  radiation ( $\lambda$  = 1.54178 Å); cell refinement was done by APEX2.<sup>45</sup> Numerical absorption corrections from face indices

were applied using SADABS,<sup>46</sup> and data reduction was done by SAINT.<sup>47</sup> SHELXTL<sup>48</sup> was used to solve and refine the structures, to manipulate the molecular graphics, and to prepare the material for publication.

**2.2. Synthesis. 2,5-Dibromo-*N,N*-dimethyl-4-nitroaniline (4).** To a stirring solution of 2,5-dibromo-4-nitroaniline (see the Supporting Information) (2.0 g, 6.74 mmol) in THF (7 mL), NaH (0.485 g, 20.2 mmol) was added slowly in small portions (~150 mg each) under positive pressure of nitrogen. MeI (4.78g, 2.10 mL, 33.68 mmol) was added via syringe. The mixture was stirred at room temperature for 2 h under a nitrogen atmosphere and monitored by TLC. Water was added to the solution, a yellow precipitate formed, and THF was removed in vacuo to ease the extraction. The reaction mixture was extracted with ethyl acetate, the organic layers were dried over sodium sulfate, and the solvents were removed in vacuo. The crude product was purified using column chromatography (dichloromethane:hexane 2:1 v/v) to obtain **4** as a yellow solid. (1.42 g, 65.3%). <sup>1</sup>H NMR (500 MHz, CDCl<sub>3</sub>): δ 8.24 (s, 1H), 7.19 (s, 1H), 2.98 (s, 6H). <sup>13</sup>C NMR (126 MHz, CDCl<sub>3</sub>): δ 155.90, 141.92, 132.52, 124.78, 115.50, 113.54, 43.45. HRMS (ESI<sup>+</sup>): calculated for C<sub>8</sub>H<sub>8</sub>Br<sub>2</sub>N<sub>2</sub>O<sub>2</sub>, 324.9005 [M + H]<sup>+</sup>; found, 324.8986 [M + H]<sup>+</sup>.

**2-Bromo-*N,N*-dimethyl-4-nitro-5-((trimethylsilyl)ethynyl)aniline (6a).** To a stirring solution of **4** (300 mg, 0.926 mmol) in THF (10 mL) at room temperature, Pd(PPh<sub>3</sub>)<sub>2</sub>Cl<sub>2</sub> (28 mg, 0.04 mmol), CuI (17.6 mg 0.09 mmol), and diisopropylamine (1.0 mL) were added sequentially. The solution turned orange-red. To this reaction mixture trimethylsilyl acetylene (99.9 mg, 0.143 mL, 1.01 mmol) was added in one portion. The solution turned dark brown. At each addition, the flask was degassed and flushed with nitrogen. The resulting reaction mixture was stirred at room temperature under nitrogen atmosphere for 1 h then filtered through Celite. The organic layer was dried in vacuo, and the resulting crude solid was purified with silica gel column chromatography using a 1:4 mixture of ethyl acetate and hexane v/v to obtain **6a** (173 mg, 55%). <sup>1</sup>H NMR (500 MHz, CDCl<sub>3</sub>): δ 8.33 (s, 1H), 7.10 (s, 1H), 2.97 (s, 6H), 0.30 (s, 9H). <sup>13</sup>C NMR (CDCl<sub>3</sub>): δ 155.50, 142.47, 131.35, 124.23, 118.77, 114.95, 104.01, 99.81, 43.31, -0.37. HRMS (ESI): calculated for C<sub>13</sub>H<sub>17</sub>BrN<sub>2</sub>O<sub>2</sub>Si, 343.0295 [M + H]<sup>+</sup>; found, 343.0278 [M + H]<sup>+</sup>.

**Dimethyl 5-((4-bromo-5-((*N,N*-dimethylamino)-2-nitrophenyl)ethynyl)isophthalate (6b).** To a stirring solution of **4** (300 mg, 0.926 mmol) and **5** (202 mg, 0.926 mmol) in THF (5 mL), Pd(PPh<sub>3</sub>)<sub>2</sub>Cl<sub>2</sub> (20 mg, 0.02 mmol), CuI (10.0 mg 0.03 mmol), and triethylamine (5.0 mL) were added in one portion sequentially. The solution turned dark brown. After each addition the flask was brought degassed and flushed with nitrogen. This mixture was stirred overnight at room temperature under a nitrogen atmosphere. Then the reaction mixture was filtered through Celite, the organic layer was dried in vacuo, and the solid was purified with silica gel column chromatography using a 4:1 mixture of dichloromethane and hexane, v/v, to obtain **6b** (220 mg, 51%). <sup>1</sup>H NMR (CDCl<sub>3</sub>): δ 8.69 (s, 1 H), 8.44 (s, 2 H), 8.43 (s, 1 H), 7.18 (s, 1 H), 3.99 (s, 6 H), 3.03 (s, 6 H). <sup>13</sup>C NMR (126 MHz, CDCl<sub>3</sub>): δ 165.43, 155.71, 141.85, 136.82, 131.77, 131.15, 130.99, 123.72, 123.52, 118.41, 115.09, 94.73, 86.92, 52.62, 43.36. HRMS (ESI): calculated for C<sub>20</sub>H<sub>17</sub>BrN<sub>2</sub>O<sub>6</sub>, 461.0343 [M + H]<sup>+</sup>; found, 461.0327 [M + H]<sup>+</sup>.

**TMS-PE(DA)-IpaOMe (7a).** A round-bottom flask was charged with **6a** (300 mg, 0.879 mmol), **5** (374 mg, 1.72

mmol), Pd(PPh<sub>3</sub>)<sub>2</sub>Cl<sub>2</sub> (12 mg, 0.017 mmol), CuI (6.5 mg 0.034 mmol), and THF (8 mL) under nitrogen atmosphere. Then diisopropylamine (0.8 mL) was added in one portion via syringe, and the solution turned dark brown. At each addition, the flask was degassed and maintained under a nitrogen atmosphere. This mixture was stirred overnight at 50 °C under nitrogen atmosphere, then cooled and filtered through Celite and a thin layer of silica gel. The organic solvent was evaporated in vacuo, and the crude solid was purified with silica gel column chromatography using a 1:2 mixture of ethyl acetate and hexane, v/v, to obtain **7a** (172 mg, 41%). <sup>1</sup>H NMR (500 MHz, chloroform-*d*): δ 8.61 (s, 1H), 8.29 (s, 2H), 8.26 (s, 1H), 6.90 (s, 1H), 3.96 (s, 6H), 3.24 (s, 6H), 0.29 (s, 9H). <sup>13</sup>C NMR (CDCl<sub>3</sub>): δ 165.68, 156.01, 140.13, 136.16, 133.01, 131.37, 130.65, 124.09, 121.17, 120.30, 110.19, 104.40, 100.88, 94.57, 89.38, 52.84, 42.95, -0.11. HRMS (ESI): calculated for C<sub>25</sub>H<sub>26</sub>N<sub>2</sub>O<sub>6</sub>Si, 479.1633 [M + H]<sup>+</sup>; found, 479.1635 [M + H]<sup>+</sup>.

**TMS-PE(AD)-IpaOMe (7b).** To a stirring solution of **6b** (330 mg, 0.72 mmol) in THF (15 mL), Pd(PPh<sub>3</sub>)<sub>2</sub>Cl<sub>2</sub> (10 mg, 0.014 mmol), CuI (5.5 mg 0.029 mmol), and diisopropylamine (7.5 mL) were added in one portion, sequentially. Then the flask was degassed, flushed with nitrogen, and trimethylsilyl acetylene (628 mg, 0.91 mL, 6.40 mmol) was added with a syringe. The solution turned dark brown. The reaction mixture was stirred overnight at 50 °C under nitrogen atmosphere. The reaction mixture was then cooled, filtered through Celite and a thin layer of silica gel, the organic layer was dried in vacuo, and the crude solid was purified with silica gel column chromatography using a 2:7 mixture of ethyl acetate and hexane, v/v to obtain **7b** (257 mg, 75%). <sup>1</sup>H NMR (500 MHz, chloroform-*d*): δ 8.68 (s, 1H), 8.43 (s, 2H), 8.29 (s, 1H), 6.94 (s, 1H), 3.98 (s, 6H), 3.23 (s, 6H), 0.28 (s, 9H). <sup>13</sup>C NMR (126 MHz, CDCl<sub>3</sub>): δ 165.47, 156.13, 138.96, 136.84, 133.46, 131.07, 130.87, 123.71, 120.22, 119.34, 110.82, 102.87, 102.55, 94.53, 87.88, 52.61, 42.62, -0.33. HRMS (ESI): calculated for C<sub>25</sub>H<sub>26</sub>N<sub>2</sub>O<sub>6</sub>Si, 479.1633 [M + H]<sup>+</sup>; found, 479.1602 [M + H]<sup>+</sup>.

**General TMS Deprotection Procedure.** To a stirring solution of **7a** or **7b** (300 mg, 0.627 mmol) in a 1:1 mixture of dichloromethane and MeOH (26 mL), K<sub>2</sub>CO<sub>3</sub> (433 mg, 3.13 mmol) was added in one portion at room temperature. The reaction mixture was stirred at room temperature, under nitrogen atmosphere for about 2.5 h and monitored by TLC for the disappearance of the starting material. Deionized water (250 mL) was added, and the product was extracted with dichloromethane (3 × 50 mL). The collected organic layers were washed with water (2 × 50 mL), dried over sodium sulfate, and the solvent was removed in vacuo. The solid crude was purified with silica gel column chromatography using a 1:2 mixture of ethyl acetate and hexane, v/v, to obtain **8a** or **8b**, respectively, as yellow solids.

**H-PE(AD)-IpaOMe 8a.** Yellow solid (204 mg, 80%). <sup>1</sup>H NMR (500 MHz, chloroform-*d*): δ 8.65 (s, 1H), 8.33 (d, *J* = 1.4 Hz, 2H), 8.32 (s, 1H), 6.97 (s, 1H), 3.98 (s, 6H), 3.56 (s, 1H), 3.26 (s, 6H). <sup>13</sup>C NMR (126 MHz, CDCl<sub>3</sub>): δ 165.45, 155.73, 139.69, 135.95, 132.97, 131.16, 130.49, 123.79, 121.35, 119.20, 110.12, 94.45, 88.99, 85.28, 79.82, 52.66, 42.71. HRMS (ESI): calculated for C<sub>22</sub>H<sub>18</sub>N<sub>2</sub>O<sub>6</sub>, 407.1238 [M + H]<sup>+</sup>; found, 407.1223 [M + H]<sup>+</sup>.

**H-PE(AD)-IpaOMe 8b.** Yellow solid (201 mg, 79%). <sup>1</sup>H NMR (500 MHz, chloroform-*d*): δ 8.68 (s, 1H), 8.43 (s, 2H),

8.32 (s, 1H), 6.97 (s, 1H), 3.98 (s, 6H), 3.51 (s, 1H), 3.22 (s, 6H).

$^{13}\text{C}$  NMR (126 MHz,  $\text{CDCl}_3$ ):  $\delta$  165.48, 156.40, 139.07, 136.88, 133.81, 131.08, 130.94, 123.65, 120.38, 119.74, 109.83, 94.68, 87.70, 84.95, 81.41, 52.63, 42.75. HRMS (ESI): calculated for  $\text{C}_{22}\text{H}_{18}\text{N}_2\text{O}_6$ , 407.1238  $[\text{M} + \text{H}]^+$ ; found, 407.1222  $[\text{M} + \text{H}]^+$ .

**ZTPP-PE(DA)-IpaOMe (1).** Zn(II) 5-(4-iodophenyl)-10,15,20-triphenylporphyrin (**9**) (300 mg, 0.373 mmol, 1 equiv), **H-PE(DA)-IpaOMe (8a)** (303 mg, 0.746 mmol, 2.0 equiv),  $\text{PdCl}_2(\text{PPh}_3)_2$  (5.24 mg, 0.0075 mmol, 0.02 equiv), and CuI (2.9 mg, 0.015 mmol, 0.04 equiv) were added to a 50 mL 2-necked round-bottom flask that was flushed with nitrogen. THF (10 mL) and diisopropyl amine (2 mL) were added via syringe under nitrogen atmosphere. The reaction was heated to 60 °C with constant stirring overnight under nitrogen. The reaction mixture was cooled to room temperature and then filtered through Celite, and the solvents were evaporated in vacuo to obtain a crude solid. It was purified with column chromatography using a 2:3 mixture of ethyl acetate and hexane, v/v to obtain **1** as a purple solid (109 mg, 27%).  $^1\text{H}$  NMR (500 MHz, chloroform-*d*):  $\delta$  9.07–8.89 (m, 8H), 8.62 (s, 1H), 8.44 (s, 1H), 8.31 (s, 2H), 8.26 (m, 8H), 8.04 (d,  $J = 7.9$  Hz, 2H), 7.78 (m, 9H), 7.15 (s, 1H), 3.97 (s, 6H), 3.34 (s, 6H).  $^{13}\text{C}$  NMR (126 MHz,  $\text{CDCl}_3$ ):  $\delta$  165.24, 155.88, 150.29, 150.23, 150.19, 149.77, 144.06, 142.79, 142.77, 139.29, 135.73, 134.69, 134.47, 133.12, 132.27, 132.09, 132.06, 131.68, 130.77, 130.33, 130.09, 127.53, 126.58, 123.73, 121.71, 121.35, 121.26, 120.59, 120.26, 119.95, 109.66, 97.66, 94.18, 89.32, 87.38, 52.54, 42.78. FT-IR-ATR:  $\nu(\text{C}-\text{H})$  2922  $\text{cm}^{-1}$ ;  $\nu(\text{C}\equiv\text{C})$  2206  $\text{cm}^{-1}$ ;  $\nu(\text{C}=\text{O})$  1728  $\text{cm}^{-1}$ ;  $\nu(\text{C}-\text{C}, \text{aromatic})$  1591  $\text{cm}^{-1}$ ;  $\nu(\text{N}-\text{O})$  1541  $\text{cm}^{-1}$ ;  $\nu(\text{C}-\text{O})$  1242  $\text{cm}^{-1}$ . HRMS (MALDI): calculated for  $\text{C}_{66}\text{H}_{44}\text{N}_6\text{O}_6\text{Zn}$ , 1080.2608  $[\text{M}]$ ; found, 1080.2619  $[\text{M}]$ .

**ZnTPP-PE(AD)-IpaOMe (3).** Zn(II) 5-(4-iodophenyl)-10,15,20-triphenylporphyrin **9** (195 mg, 0.242 mmol, 1.0 equiv), **H-PE(AD)-IpaOMe (8b)** (197 mg, 0.485 mmol, 2.0 equiv),  $\text{PdCl}_2(\text{PPh}_3)_2$  (3.4 mg, 0.004 mmol, 0.02 equiv), and CuI (2 mg, 0.0095 mmol, 0.04 equiv) were dissolved in anhydrous THF (10 mL), and the solution was flushed with nitrogen. Diisopropylamine (2 mL) was added in one portion, and the reaction mixture was heated at 60 °C overnight under nitrogen atmosphere. The resulting solution was allowed to cool to room temperature and then filtered through Celite, and the solvents were removed in vacuo. The dark brown crude was purified with silica gel column chromatography using a 2:3 mixture of ethyl acetate and hexane, v/v, to obtain **3** as a purple solid (121 mg, 46%).  $^1\text{H}$  NMR (500 MHz, chloroform-*d*):  $\delta$  8.98 (m, 8H), 8.69 (s, 1H), 8.52 (s, 1H), 8.47 (s, 2H), 8.40–8.07 (m, 8H), 7.93 (d,  $J = 5.2$  Hz, 2H), 7.77 (m, 9H), 7.08 (s, 1H), 3.99 (s, 6H), 3.43 (s, 6H).  $^{13}\text{C}$  NMR (126 MHz,  $\text{CDCl}_3$ ):  $\delta$  165.49, 155.98, 150.33, 150.30, 150.20, 149.77, 143.63, 142.71, 139.40, 136.87, 134.64, 134.43, 132.91, 132.26, 132.15, 132.10, 131.61, 131.06, 130.87, 129.40, 127.57, 126.59, 123.76, 121.97, 121.45, 121.32, 120.42, 119.89, 119.23, 111.35, 97.10, 94.64, 88.39, 88.00, 52.62, 42.85. FT-IR-ATR:  $\nu(\text{C}-\text{H})$  2924  $\text{cm}^{-1}$ ;  $\nu(\text{C}\equiv\text{C})$  2218  $\text{cm}^{-1}$ ;  $\nu(\text{C}=\text{O})$  1730  $\text{cm}^{-1}$ ;  $\nu(\text{C}-\text{C}, \text{aromatic})$  1595  $\text{cm}^{-1}$ ;  $\nu(\text{N}-\text{O})$  1541  $\text{cm}^{-1}$ ;  $\nu(\text{C}-\text{O})$  1236  $\text{cm}^{-1}$ . HRMS (MALDI): calculated for  $\text{C}_{66}\text{H}_{44}\text{N}_6\text{O}_6\text{Zn}$ , 1080.2608  $[\text{M}]$ ; found, 1080.2577  $[\text{M}]$ .

**General Hydrolysis Procedure.** Ester **1** (42 mg, 0.04 mmol) or ester **3** (52.5 mg, 0.05 mmol) was dissolved in a mixture of THF and methanol (1:1 ratio, 4 mL). A 2 N NaOH aqueous

solution (5 mL, 10 mmol) was then added, and the reaction mixture was stirred for 3 h at reflux (87 °C). After the reaction was completed (TLC) organic solvents were removed in vacuo. The unreacted ester was extracted using chloroform, and the carboxylate salt remained in the water layer as a fine suspension. The aqueous layer was then acidified by cautious, dropwise addition of 2 N HCl aqueous to pH  $\sim$  3. The fine solid was collected by vacuum filtration on a 0.45  $\mu\text{m}$  PTFE filter and washed with copious amounts of water to yield a purplish-brown solid:

**ZnTPP-DA-Ipa (1-acid).** 33 mg, 79%.  $^1\text{H}$  NMR (THF-*d*<sub>8</sub>):  $\delta$  10.82 (s, 1H, carboxylic acid), 8.88 (m, 4H), 8.84 (s, 4H), 8.66 (s, 1H), 8.45 (s, 1H), 8.39 (s, 2H), 8.27 (d,  $J = 7.8, 2\text{H}$ ), 8.20 (m, 6H), 8.01 (d,  $J = 7.4, 2\text{H}$ ), 7.75 (d,  $J = 5.6, 9\text{H}$ ), 7.28 (s, 1H), 3.37 (s, 6H). FT-IR-ATR:  $\nu(\text{O}-\text{H})$  weak 3500–3000  $\text{cm}^{-1}$ ;  $\nu(\text{C}-\text{H})$  2924  $\text{cm}^{-1}$ ;  $\nu(\text{C}\equiv\text{C})$  2208  $\text{cm}^{-1}$ ;  $\nu(\text{C}=\text{O})$  1714  $\text{cm}^{-1}$ ;  $\nu(\text{C}-\text{C}, \text{aromatic})$  1593  $\text{cm}^{-1}$ ;  $\nu(\text{N}-\text{O})$  1541  $\text{cm}^{-1}$ ;  $\nu(\text{C}-\text{O})$  1259  $\text{cm}^{-1}$ .

**ZnTPP-AD-Ipa (3-acid).** 27 mg, 53%.  $^1\text{H}$  NMR (500 MHz, THF-*d*<sub>8</sub>):  $\delta$  8.95–8.86 (m, 4H), 8.85 (s, 4H), 8.69 (s, 1H), 8.47 (s, 1H), 8.44 (s, 2H), 8.27 (d,  $J = 7.8$  Hz, 2H), 8.21 (d,  $J = 7.0$  Hz, 6H), 7.97 (d,  $J = 7.8$  Hz, 2H), 7.75 (d,  $J = 6.2$  Hz, 9H), 7.25 (s, 9H), 3.42 (s, 6H). FT-IR-ATR:  $\nu(\text{O}-\text{H})$  weak 3500–3000  $\text{cm}^{-1}$ ;  $\nu(\text{C}-\text{H})$  2926  $\text{cm}^{-1}$ ;  $\nu(\text{C}\equiv\text{C})$  2198  $\text{cm}^{-1}$ ;  $\nu(\text{C}=\text{O})$  1699  $\text{cm}^{-1}$ ;  $\nu(\text{C}-\text{C}, \text{aromatic})$  1597  $\text{cm}^{-1}$ ;  $\nu(\text{N}-\text{O})$  1543  $\text{cm}^{-1}$ ;  $\nu(\text{C}-\text{O})$  1261  $\text{cm}^{-1}$ .

**2.3. X-ray Crystal Structure Determination.** ORTEP diagrams with the numbering schemes of the crystal structures of (**8a**), (**8b**), and (**1**) are shown in Figures 2 and 3.

**For (8a).** A yellow plate of  $\text{C}_{22}\text{H}_{18}\text{N}_2\text{O}_6$  was obtained by slow evaporation from THF. Unit cell parameters were determined by least-squares refinement of 6246 reflections between  $\theta$  of 3.18 and 72.07°. Intensity data were collected, integrated, and corrected for absorption as well as Lorentz and polarization. Standard procedures and programs were used to solve and refine the structure.<sup>45–48</sup> There were a total of 18872 reflections and 3492 independent observations. The solution was found by direct methods. The final refinement on  $F^2$  involved an anisotropic model for all nonhydrogen atoms. All the H atoms were found in electron-density difference maps and were then placed as riding models on their respective C atoms. With 275 parameters, the refinement converged to a conventional R value of 5.3%. Cell dimensions and all of the metrical data are shown in Table S1 of the Supporting Information. Planes and angles for the selected atoms are given in Table S2 of the Supporting Information.

**For (8b).** A yellow plate of  $\text{C}_{22}\text{H}_{18}\text{N}_2\text{O}_6$  was obtained from THF. Cell dimensions, data, etc., were handled exactly as above. Unit cell parameters were determined by least-squares refinement of 9837 reflections between  $\theta$  of 3.55 and 71.68°. There were a total of 15006 reflections and 3454 independent observations. With 275 parameters, the refinement converged to a conventional R value of 4.4%. Cell dimensions and the metrical data are also shown in Table S1 of the Supporting Information. Planes and angles for the selected atoms are given in Table S2 of the Supporting Information.

**For (1).** A red plate of  $\text{C}_{74}\text{H}_{60}\text{N}_6\text{O}_8\text{Zn}$  was obtained from THF. Cell dimensions, data, etc., were accumulated exactly as above. Unit cell parameters were determined by least-squares refinement of 9993 reflections between  $\theta$  of 2.77 and 69.31°. There were a total of 29037 reflections and 17401 independent observations. The structure was solved in the space group P1, with 2 molecules in the asymmetric unit; there are two THF

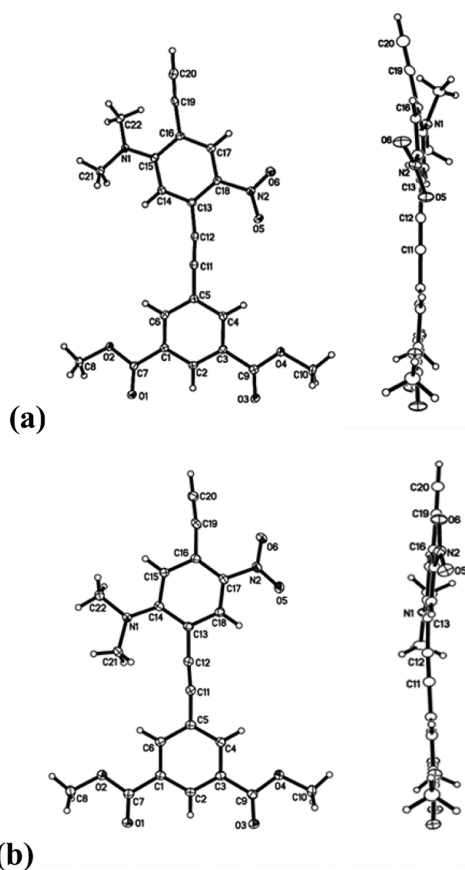


**Figure 2.** X-ray crystal structure of (a) H-PE(DA)-IpaOMe (**8a**) and (b) H-PE(AD)-IpaOMe (**8b**). Left: front-view showing the distortion of the backbone. Right: the respective edge-on views showing the nonlinearity of the whole molecule; planes and angles for the named atoms are given in Table S2 of the Supporting Information.

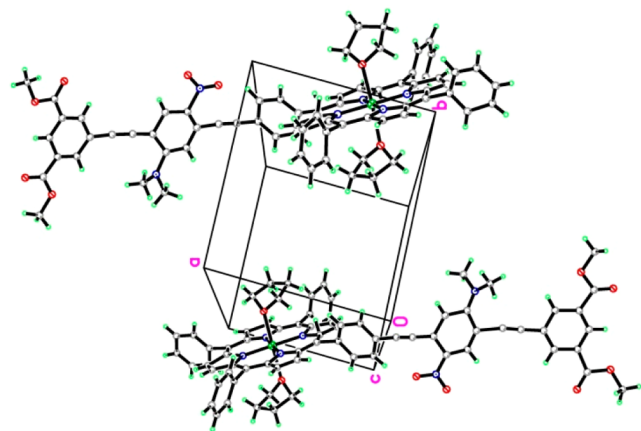


**Figure 3.** X-ray crystal structure of ZnTPP-PE(DA)-IpaOMe (**1**).

molecules bonded to each Zn ion. There are also 5 THF molecules of crystallization (mostly disordered, even at 100 K) associated with these molecules; these were handled with the program SQUEEZE.<sup>49</sup> This removed the disordered THF solvent molecules from the structure. These solvent molecules cause the symmetry between the two molecules to be pseudosymmetric and the space group to be almost  $P\bar{1}$ ; however, there was enough disorder in the THF molecules to destroy this symmetry. With 1432 parameters, the refinement converged to a conventional  $R$  value of 12.1%. The crystal is

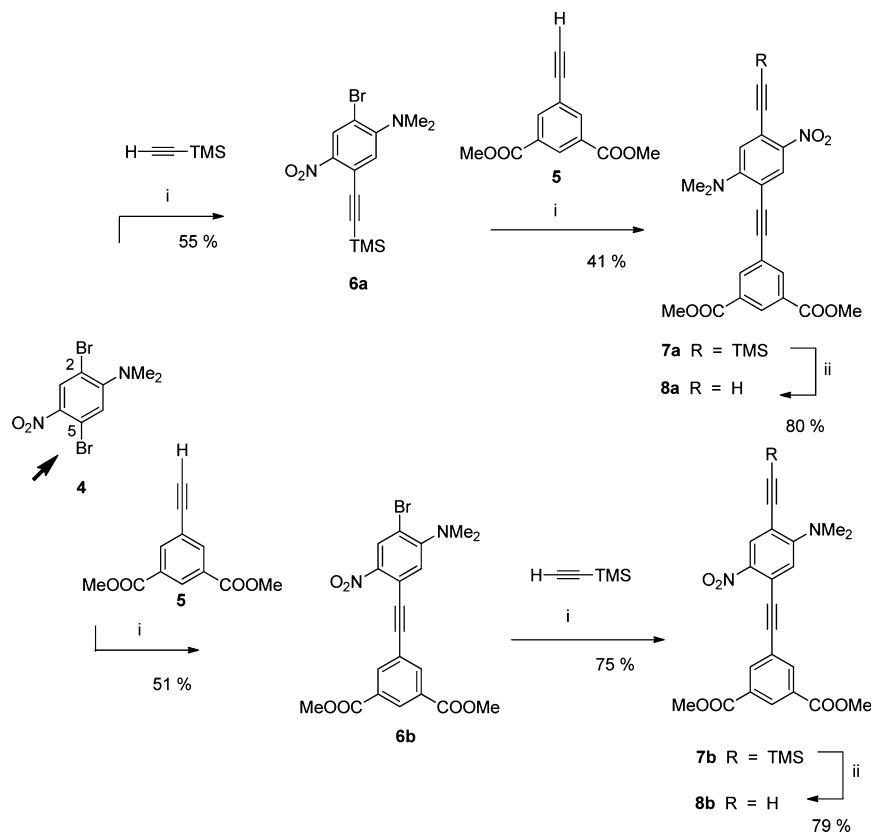
also twinned, with a twinning ratio 0.66:0.34(6). Cell dimensions and the metrical data are also shown in Table S1 of the Supporting Information. Planes and angles for the selected atoms are given in Table S2 of the Supporting Information.

### 3. RESULTS AND DISCUSSION

**3.1. Synthesis.** The synthesis of the rigid rod porphyrins **1** and **3**, illustrated in Schemes 1 and 2, followed the general strategy previously reported for **2**,<sup>28</sup> which involves a series of Pd-catalyzed cross-coupling reactions. The modular approach involved a 3-step procedure in which previously synthesized building blocks were assembled to yield **1** and **3** in 5% and 14% total yield from **4**, respectively. A requirement for the synthesis of porphyrins **1** and **3** was the ability to introduce the internal dipole in the linker unit by functionalizing the central phenyl moiety with an electron donor and an acceptor group in para position with respect to each other and to be able to switch the position of these groups with respect to the Ipa anchor unit.

This was accomplished by using *N,N*-dimethyl-2,5-dibromo-4-nitroaniline (**4**) as the precursor to the central unit of the linker. 2,5-Dibromo-4-nitroaniline was reported to exhibit enhanced reactivity of the bromine in ortho to the nitro group in Pd catalyzed cross-coupling reactions with alkynes, a property that we anticipated would be retained by the *N,N*-dimethyl derivative, **4**. The amine was methylated to enhance the electron donation ability of the amino group. The enhanced reactivity of the bromine in ortho to the nitro group [Br(5), indicated with an arrow in Scheme 1] allowed for the regioselective coupling either with trimethylsilyl (TMS) acetylene to form **6a**, leaving Br(2) available for introduction of the anchor Ipa unit, or to couple it directly with the anchor Ipa unit to form **6b**, leaving Br(2) available for reaction with TMS acetylene, for subsequent coupling with the ZnTPP chromophore. In summary, the reversal of the donor and acceptor positions on the linker was obtained by reversing the position of the anchor and the chromophore on the linker unit on precursor **4**. The two sequences are shown in Scheme 1. Methyl esters **1–3** were used for solution characterization and spectral studies (UV-vis, fluorescence) because they exhibited good solubility in organic solvents and were hydrolyzed to the corresponding carboxylic acids for binding to metal oxide semiconductors. Whereas samples of **1** and **3** exhibited some degradation over time, depending on the storage conditions (vide infra), no changes were observed for samples of **2** stored for years, suggesting that **2** is chemically more stable than **1** and **3**.

**3.2. Single Crystal X-ray Structure.** Crystals of **8a**, **8b**, and **1** (see Figure 2, Figure 3, and Supporting Information) were obtained from THF solutions either cold or at room temperature. The crystals of **1** were obtained by storing the THF solution cold (about 4 °C). Crystals of **8a** and **8b** were also obtained from ethyl acetate/hexane or dichloromethane but were not of satisfactory quality for single crystal X-ray structure. The crystal structures of **8a** and **8b** confirmed the dipole reversal and show significant distortions both along the molecular backbone [C1–C2–C3–C4–C5–C6 vs C13–C16–C19–C20] (“twist” angle = 17.04 deg for **8a** and 7.01 deg for **8b**) and of the plane of the molecule (14.4 deg for **8a** and 8.7 deg for **8b**) ascribed to crystal packing and/or the presence of the nitro and *N,N*-dimethylamino substituents on the phenyl ring. Both types of distortions are evident in Figure 2 through the front-view and edge-on-view of the two

Scheme 1. Synthesis of Dipole-Containing Linkers H-PE(DA)-IpaOMe (**8a**) and H-PE(AD)-IpaOMe (**8b**)<sup>a</sup>

<sup>a</sup>Reagents and conditions: (i)  $\text{Pd}(\text{PPh}_3)_2\text{Cl}_2$ ,  $\text{CuI}$ ,  $(i\text{Pr})_2\text{NH}$ , THF and (ii) (a)  $\text{K}_2\text{CO}_3$ ,  $\text{CH}_2\text{Cl}_2$ , MeOH 2.5 h, rt. (b) HCl.

molecules. We believe that the nitro group in the ortho position in (**8a**) exhibits electronic repulsion of the C11–C12 acetylenic bond (the distance of O5 to C12 is only 2.69 Å), leading to the nonlinearity of the molecule as a whole; the “tilt” angle [defined by the angle C11–C2–C16] is  $\sim 3.7$  deg for **8a**, as shown in Figure 2a. In **8b**, the nitro group is far removed from the same acetylenic moiety, and therefore, there is less distortion of the molecule; the same “tilt” angle is  $\sim 2.4$  deg, as shown in Figure 2b. The crystal packing of **8a** and **8b**, shown in Figure S31 of the Supporting Information and Figure S32 of the Supporting Information, respectively, differ considerably: in molecule **8a**, all of the nitro groups in 1/2 of the cell point toward the *a* cell direction and in the other 1/2 of the cell (by symmetry), these nitro groups point in the  $-a$  cell direction. In **8b**, the nitro groups alternate throughout the cell going toward the *b* cell direction and then toward the  $-b$  cell direction, and then toward the *b* direction again. It seems that there is more of an antiparallel orientation of the dipole for **8a** than for **8b**. Given the distances between the molecular planes in the lattice ( $\sim 3.8$  Å), however, it is unlikely that dipole–dipole interactions are responsible for this arrangement.

The crystal structure of **1** in Figure 3 shows the presence of large channels in the lattice that were filled with about five molecules of the crystallization solvent (THF). The axial coordination of the central zinc metal ion with two THF molecules and an antiparallel arrangement of the internal molecular dipoles are also evident. There is  $\sim 4.5$  Å between molecules, leaving a large channel to accommodate the THF molecules. The space group is *P1* but is very close to being the centrosymmetric *P1*; the presence of the THF molecules

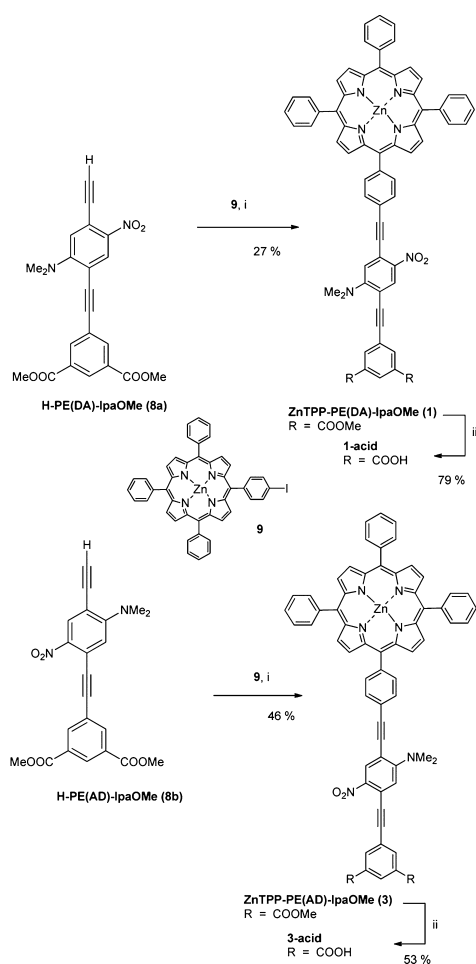
reduces the symmetry to being that of the noncentrosymmetric space group.

### 3.3. Spectroscopic and Electrochemical Properties.

The UV–vis absorption and emission spectra of acetonitrile solutions of **1**, **2**, and **3** were recently reported,<sup>27</sup> and these data are overlaid in Figure 4 (panels a and c, respectively) and compared with the spectra of the linker units in Figure 4b.

The UV–vis spectra of the linkers containing the D and A substituents exhibited an additional absorption band centered at 407 nm for **8a** and 396 nm for **8b**, compared to the linker without substituents. The shift is not surprising as the dipole reversal with respect to the Ipa unit occurs in a highly conjugated system. The UV–vis spectra of **1**, **2**, and **3** exhibited characteristic features of the ZnTPP chromophore, with bands centered at 422 nm (Soret), 556 and 597 nm (Q bands), in addition to higher energy bands assigned to the  $\pi-\pi^*$  transitions of the PE conjugated bridge. The steady-state fluorescence emission spectra exhibited two bands at 603 and 656 nm, which are consistent with the Q(0,0) and Q(1,0) vibrational states transitions observed for the ZnTPP macrocycle.

Cyclic voltammetry was performed on the methyl esters **1–3** because of their solubility in organic solvents and to prevent physisorption and decarboxylation processes usually associated with the carboxylic acids.<sup>28</sup> The electrochemical properties were studied in dichloromethane with 0.1 M  $\text{Bu}_4\text{NBF}_4$  supporting electrolyte and were referenced to saturated calomel electrode (SCE). Porphyrins **1–3** exhibited very similar redox behavior, consistent with that of ZnTPP porphyrins,<sup>28</sup> and with the first and second oxidation reversible and in the same ranges (see Table 1).

Scheme 2. Synthesis of 1 and 3 and Hydrolysis to the Corresponding Carboxylic Acids<sup>a</sup>

<sup>a</sup>Reagents and conditions: (i) Pd(PPh<sub>3</sub>)<sub>2</sub>Cl<sub>2</sub>, CuI, (iPr)<sub>2</sub>NH, THF and (ii) 6 N NaOH in MeOH, CH<sub>2</sub>Cl<sub>2</sub>, 3h.

In summary, the electrochemical and spectroscopic properties for 1, 2, and 3 are virtually indistinguishable, indicating that the ZnTPP chromophore properties are not affected by the functionalization of the linker with the donor and acceptor groups or by the dipole reversal. As described in Introduction, this was expected since the ZnTPP chromophore is electronically decoupled from substituents on the meso phenyl rings. In particular, the data indicate that the energy gap between excited states and ground states are the same for all three compounds. It is worth noticing that a small, broad shoulder centered at about 635 nm in the absorption spectra was observed for solid samples of 1 and 3 stored for several months at room temperature and exposed to light. The shoulder band was completely suppressed by adding a few drops of a ZnOAc<sub>2</sub> MeOH solution, suggesting that it was related to the presence of free porphyrins that could be metallized again.

#### 4. CONCLUSIONS

Rigid-rod Zn(II) tetraphenylporphyrins (ZnTPP) 1 and 3, containing an intramolecular dipole in the linker, were synthesized in a modular approach and were compared to the previously reported 2, which is identical in structure but does not contain substituents in the linker. The dipole was obtained by introducing electron donor (*N,N*-dimethylamino) and

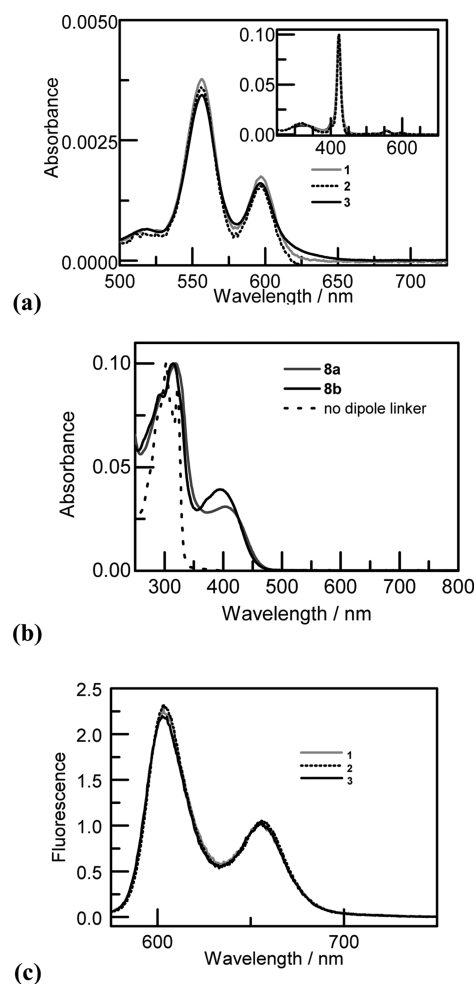


**Figure 4.** (a) Expanded Q-band region of the UV-vis absorption spectra for 1, 2, and 3 measured in acetonitrile normalized to 0.1 at 423 nm. Inset: UV-vis absorption spectra for 1, 2, and 3. Adapted from data reported in ref 27. (b) Absorption spectra of three linker molecules in acetonitrile. (c) Fluorescence emission spectra normalized at 603 nm for 1, 2, and 3 in acetonitrile ( $\lambda_{\text{exc}} = 556$  nm). Adapted from data reported in ref 27.

**Table 1. Solution Redox Potentials of 1-3 in Dichloromethane Reported vs SCE<sup>a</sup>**

porphyrin	oxidation (V)	
	1st	2nd
1	0.87	1.15
2	0.86	1.14
3	0.85	1.15

<sup>a</sup>All cyclic voltammograms were measured at a scan rate of 50 mV s<sup>-1</sup> using a glassy carbon working electrode

withdrawing (nitro) groups in the central phenyl ring of the linker, and the dipole reversal was achieved by switching the position of the two groups. The UV-vis and steady-state emission properties of the dipole-containing ZnTPP compounds 1, 2, and 3 were identical. The X-ray crystal structure of the linker units shows a distortion due to the presence of the nitro and *N,N*-dimethylamino substituents on the central phenyl ring, but the orientation of the molecules in the packing does not seem to be influenced by the presence of internal dipoles. Compounds 1-3 were studied to demonstrate the

influence of a molecular dipole on the energy level alignment of a chromophore bound to a metal oxide semiconductor,<sup>27</sup> and time-resolved electron transfer studies of 1–3 bound to TiO<sub>2</sub> nanoparticle films to determine the influence of such dipoles on charge transfer kinetics are currently in progress.

## ■ ASSOCIATED CONTENT

### ■ Supporting Information

Synthetic procedures for the synthesis of 2,5-dibromo-4-nitroaniline; <sup>1</sup>H and <sup>13</sup>C NMR and HRMS (ESI or MALDI) for 4, 6a, 6b, 7a, 7b, 8a, 8b, 1, 3, 1-acid, 3-acid; and FTIR-ATR spectra of compounds 1, 3, 1-acid, and 3-acid; tables with cell dimensions, angles, and all of the metrical data for crystal structures of 8a, 8b, and 1; and packing diagrams of 8a and 8b. This material is available free of charge via the Internet at <http://pubs.acs.org>.

## ■ AUTHOR INFORMATION

### Corresponding Author

\*E-mail: galoppin@rutgers.edu.

### Notes

The authors declare no competing financial interest.

## ■ ACKNOWLEDGMENTS

The authors are grateful to Prof. Jonathan Rochford for assistance with the CV measurements and to Dr. Sylvie Rangan for discussions about the dipole effect. Funding by the Division of Chemical Sciences, Geosciences, and Biosciences, Office of Basic Energy Sciences of the U.S. Department of Energy through Grant DE-FG02-01ER15256 is gratefully acknowledged. A.B. thanks Rutgers University for the Summer 2013 FASN Dean's Undergraduate Research Fellowship and the Chemistry Department for the 2014 Ian Fryer Memorial Award.

## ■ REFERENCES

- (1) Cahen, D.; Kahn, A. Electron energetics at surfaces and interfaces: Concepts and experiments. *Adv. Mater.* **2003**, *15*, 271–277.
- (2) Greiner, M. T.; Helander, M. G.; Tang, W.-M.; Wang, Z.-B.; Qiu, J.; Lu, Z.-H. Universal energy-level alignment of molecules on metal oxides. *Nat. Mater.* **2012**, *11*, 76–81.
- (3) Heimel, G.; Rissner, F.; Zojer, E. Modeling the electronic properties of pi-conjugated self-assembled monolayers. *Adv. Mater.* **2010**, *22*, 2494–2513.
- (4) Hwang, J.; Wan, A.; Kahn, A. Energetics of metal-organic interfaces: New experiments and assessment of the field. *Mater. Sci. Eng.* **2009**, *R64*, 1–31.
- (5) Ishii, H.; Sugiyama, K.; Ito, E.; Seki, K. Energy level alignment and interfacial electronic structures at organic/metal and organic/organic interfaces. *Adv. Mater.* **1999**, *11*, 605–625.
- (6) Kahn, A.; Koch, N.; Gao, W. Y. Electronic structure and electrical properties of interfaces between metals and pi-conjugated molecular films. *J. Polym. Sci., Polym. Phys.* **2003**, *41*, 2529–2548.
- (7) Koch, N. Electronic structure of interfaces with conjugated organic materials. *Phys. Status Solidi RRL* **2012**, *6*, 277–293.
- (8) Vazquez, H.; Flores, F.; Kahn, A. Induced Density of States model for weakly-interacting organic semiconductor interfaces. *Org. Electron.* **2007**, *8*, 241–248.
- (9) Lindell, L.; Çakır, D.; Brocks, G.; Fahlman, M.; Braun, S. Role of intrinsic molecular dipole in energy level alignment at organic interfaces. *Appl. Phys. Lett.* **2013**, *102*, 223301.
- (10) Demirkan, K.; Mathew, A.; Weiland, C.; Yao, Y.; Rawlett, A. M.; Tour, J. M.; Opila, R. L. Energy level alignment at organic semiconductor/metal interfaces: Effect of polar self-assembled monolayers at the interface. *J. Chem. Phys.* **2008**, *128*, 074705.
- (11) Holm, A. H.; Ceccato, M.; Donkers, R. L.; Fabris, L.; Pace, G.; Maran, F. Effect of peptide ligand dipole moments on the redox potentials of Au38 and Au140 Nanoparticles. *Langmuir* **2006**, *22*, 10584–10589.
- (12) De Angelis, F.; Fantacci, S.; Selloni, A.; Grätzel, M.; Nazeeruddin, M. K. Influence of the sensitizer adsorption mode on the open-circuit potential of dye-sensitized solar cells. *Nano Lett.* **2007**, *7*, 3189–3195.
- (13) Arnaud, G. F.; De Renzi, V.; del Pennino, U.; Biagi, R.; Corradini, V.; Calzolari, A.; Ruini, A.; Catellani, A. Nitrocatechol/ZnO interface: The role of dipole in a dye/metal-oxide model system. *J. Phys. Chem. C* **2014**, *118*, 3910–3917.
- (14) Becucci, L.; Guryanov, I.; Maran, F.; Guidelli, R. Effect of a strong interfacial electric field on the orientation of the dipole moment of thiolated Aib-oligopeptides tethered to mercury on either the N- or C-Terminus. *J. Am. Chem. Soc.* **2010**, *132*, 6194–6204.
- (15) Bartucci, A.; Florián, J.; Cizek, J. W. Spectroscopic evidence of work function alterations due to photoswitchable monolayers on gold surfaces. *J. Phys. Chem. C* **2013**, *117*, 19471–19476.
- (16) Evans, S. D.; Ulman, A. Surface Potential studies of alkyl-thiol monolayers adsorbed on gold. *Chem. Phys. Lett.* **1990**, *170*, 462–466.
- (17) Imanishi, Y.; Miura, Y.; Iwamoto, M.; Kimura, S.; Umemura, J. Surface potential generation by helical peptide monolayers and multilayers on gold surface. *Proc. Jpn. Acad., Ser. B* **1999**, *75*, 287–290.
- (18) Risko, C.; Zangmeister, C. D.; Yao, Y.; Marks, T. J.; Tour, J. M.; Ratner, M. A.; van Zee, R. D. Experimental and theoretical identification of valence energy levels and interface dipole trends for a family of (oligo)phenylene-ethynylene-thiols adsorbed on gold. *J. Phys. Chem. C* **2008**, *112*, 13215–13222.
- (19) Yasutomi, S.; Morita, T.; Imanishi, Y.; Kimura, S. A Molecular photodiode system that can switch photocurrent direction. *Science* **2004**, *304*, 1944–1947.
- (20) Goh, C.; Scully, S. R.; McGehee, M. D. Effects of molecular interface modification in hybrid organic-inorganic photovoltaic cells. *J. Appl. Phys.* **2007**, *101*, 114503–114512.
- (21) Cho, C.-P.; Chu, C.-C.; Chen, W.-T.; Huang, T.-C.; Tao, Y.-T. Molecular modification on dye-sensitized solar cells by phosphonate self-assembled monolayers. *J. Mater. Chem.* **2012**, *22*, 2915–2921.
- (22) Kusama, H.; Arakawa, H. Influence of pyrimidine additives in electrolytic solution on dye-sensitized solar cell performance. *J. Photochem. Photobiol., A* **2003**, *160*, 171–179.
- (23) Ruhle, S.; Greenshtein, M.; Chen, S. G.; Merson, A.; Pizem, H.; Sukeinik, C. S.; Cahen, D.; Zaban, A. Molecular adjustment of the electronic properties of nanoporous electrodes in dye-sensitized solar cells. *J. Phys. Chem. B* **2005**, *109*, 18907.
- (24) Krueger, J.; Bach, U.; Graetzel, M. Modification of TiO<sub>2</sub> heterojunctions with benzoic acid derivatives in hybrid molecular solid-state devices. *Adv. Mater.* **2000**, *12*, 447–451.
- (25) Tada, A.; Geng, Y.; Wei, Q.; Hashimoto, K.; Tajima, K. Tailoring organic heterojunction interfaces in bilayer polymer photovoltaic devices. *Nat. Mater.* **2011**, *10*, 450–455.
- (26) Cappel, U. B.; Plogmaker, S.; Johansson, E. M. J.; Hagfeldt, A. Energy alignment and surface dipoles of rylene dyes adsorbed to TiO<sub>2</sub> nanoparticles. *Phys. Chem. Chem. Phys.* **2011**, *13*, 14767–14774.
- (27) Rangan, S.; Batarseh, A.; Chitre, K. P.; Kopecky, A.; Galoppini, E.; Bartynski, R. A. Tuning energy level alignment at organic/semiconductor interfaces using a built-in dipole in chromophore-bridge-anchor compounds. *J. Phys. Chem. C* **2014**, *118*, 12923–12928.
- (28) Rochford, J.; Galoppini, E. Zinc(II) tetraarylporphyrins anchored to TiO<sub>2</sub>, ZnO, and ZrO<sub>2</sub> nanoparticle films through rigid-rod linkers. *Langmuir* **2008**, *24*, 5366–5374.
- (29) Rochford, J.; Chu, D.; Hagfeldt, A.; Galoppini, E. Tetrachelate porphyrin chromophores for metal oxide semiconductor sensitization: Effect of the spacer length and anchoring group position. *J. Am. Chem. Soc.* **2007**, *129*, 4655–4665.
- (30) Rangan, S.; Coh, S.; Bartynski, R. A.; Chitre, K. P.; Galoppini, E.; Jaye, C.; Fischer, D. Energy alignment, molecular packing, and electronic pathways: Zinc(II) Tetraphenylporphyrin derivatives

adsorbed on TiO<sub>2</sub>(110) and ZnO(11–20) Surfaces. *J. Phys. Chem. C* **2012**, *116*, 23921–23930.

(31) Rangan, S.; Katalinic, S.; Thorpe, R.; Bartynski, R. A.; Rochford, J.; Galoppini, E. Energy level alignment of a Zinc(II) tetraphenylporphyrin dye adsorbed onto TiO<sub>2</sub>(110) and ZnO(11–20) surfaces. *J. Phys. Chem. C* **2010**, *114*, 1139–1147.

(32) Campbell, W. M.; Burrell, A. K.; Officer, D. L.; Jolley, K. W. Porphyrins as light harvesters in the dye-sensitized TiO<sub>2</sub> solar cell. *Coord. Chem. Rev.* **2004**, *248*, 1363–1379.

(33) Yella, A.; Lee, H. W.; Tsao, H. N.; Yi, C. Y.; Chandiran, A. K.; Nazeeruddin, M. K.; Diau, E. W. G.; Yeh, C. Y.; Zakeeruddin, S. M.; Grätzel, M. Porphyrin-sensitized solar cells with cobalt (II/III)-based redox electrolyte exceed 12% efficiency. *Science* **2011**, *334*, 629–634.

(34) Li, L.-L.; Diau, E. W.-G. Porphyrin-sensitized solar cells. *Chem. Soc. Rev.* **2013**, *42*, 291–304.

(35) Imahori, H.; Kurotobi, K.; Walter, M. G.; Rudin, A. B.; Wamser, C. C. Porphyrin- and Phthalocyanine-Based Solar Cells. In *Handbook of Porphyrin Science*; Kadish, K. M., Smith, K. M., Guillard, R., Eds.; World Scientific: Singapore, 2012; Chapter 13, pp 349–374.

(36) Wang, C.-L.; Hu, J.-Y.; Wu, C.-H.; Kuo, H.-H.; Chang, Y.-C.; Lan, Z.-J.; Wu, H.-P.; Diau, E. W.-G.; Lin, C.-Y. Highly efficient porphyrin-sensitized solar cells with enhanced light harvesting ability beyond 800 nm and efficiency exceeding 10%. *Energy Environ. Sci.* **2014**, *7*, 1392–1396.

(37) Lin, C.-Y.; Lo, C.-F.; Luo, L.; Lu, H.-P.; Hung, C.-S.; Diau, E. W.-G. Design and Characterization of Novel Porphyrins with Oligo(phenylethynyl) Links of Varied Length for Dye-Sensitized Solar Cells: Synthesis and Optical, Electrochemical, and Photovoltaic Investigation. *J. Phys. Chem. C* **2009**, *113*, 755–764.

(38) *Multiporphyrin Arrays: Fundamentals and Applications*, Kim, D., Ed.; Pan Stanford Publishing: Singapore, 2012.

(39) Lazarides, T.; Delor, M.; Sazanovich, I. V.; McCormick, T. M.; Georgakaki, I.; Charalambidis, G.; Weinstein, J. A.; Coutsolelos, A. G. Photocatalytic hydrogen production from a noble metal free system based on a water soluble porphyrin derivative and a cobaloxime catalyst. *Chem. Commun.* **2014**, *50*, 521–523.

(40) Youngblood, W. J.; Anna Lee, S.-H.; Maeda, K.; Mallouk, T. E. Visible light water splitting using dye-sensitized oxide semiconductors. *Acc. Chem. Res.* **2009**, *42*, 1966–1973.

(41) Gust, D.; Moore, T. A.; Moore, A. L. Mimicking photosynthetic solar energy transduction. *Acc. Chem. Res.* **2001**, *34*, 40–48.

(42) Mathew, S.; Imahori, H. Application of Multiporphyrin Arrays to Solar Energy Conversion. In *Multiporphyrin Arrays*; Kim, D., Ed.; Pan Stanford Publishing: Singapore, 2012; Chapter 9, pp 439–498.

(43) Moroni, M.; Le Moigne, J.; Pham, T. A.; Bigot, J.-Y. Rigid Rod Conjugated Polymers for Nonlinear Optics. 3. Intramolecular H bond effects on poly(phenyleneethynylene) chains. *Macromolecules* **1997**, *30*, 1964–1972.

(44) Wang, C.; Batsanov, A. S.; Bryce, M. R.; Sage, I. An improved synthesis and structural characterization of 2-(4-acetylthiophenylethynyl)-4-nitro-5-phenylethynylaniline: The molecule showing high negative differential resistance (NDR). *Synthesis* **2003**, 2089–2095.

(45) *Bruker APEX 2*, version 2.0–2; Bruker AXS Inc.: Madison, Wisconsin, 2006.

(46) Sheldrick, G. M. *SADABS*; University of Gottingen: Germany, 2008.

(47) *Bruker SAINT*, version 7.23a; Bruker AXS Inc.: Madison, Wisconsin, 2005.

(48) Sheldrick, G. M. A short history of SHELX. *Acta Cryst. A* **2008**, *64*, 112–122.

(49) Spek, A. L. Structure validation in chemical crystallography. *Acta Cryst. D* **2009**, *65*, 148–155.